Journal of Solid State Chemistry **156,** 207–212 (2001)
doi:10.1006/jssc.2000.8983, available online at http://www.idealibrary.com on IDEAL®

X-ray Structure Refinements and Strain Analysis of Substituted Cubic Lead Pyrochlores $Pb_2(M_{2-y}Pb_y)O_{7-\delta}$ ($0.0 < y < 0.8$; M = Nb or Ta)

G. Nalini,* R. Somashekar,† and T. N. Guru Row*,[1]

*Solid State and Structural Chemistry Unit, Indian Institute of Science, Bangalore 560 012, India; and †Department of Studies in Physics, University of Mysore, Mysore 570006, India

Received June 20, 2000; in revised form September 1, 2000; accepted October 3, 2000; published online December 21, 2000

The phase diagrams in the $PbO–Nb_2O_5$ system and the $PbO–Ta_2O_5$ system depict pyrochlore structure at certain molar ratios. Compositions $Pb_2Nb_{1.51}Pb_{0.49}O_{6.30}$ (1), $Pb_2Ta_{1.4}Pb_{0.6}O_{6.21}$ (2), and $Pb_2Ta_{1.25}Pb_{0.75}O_{6.57}$ (3) belonging to this family, are refined in the cubic space group $Fd\bar{3}m$ ($Z = 8$; lattice parameter $a = 10.762(1)$, 10.744(1), 10.757(5) Å, respectively) using the Rietveld refinement approach. The analyses suggest that the B-site is partially occupied by Pb leading to the general formula $Pb_2(M_{2-y}Pb_y)O_{7-\delta}$ ($0.0 < y < 0.8$; M = Nb or Ta). There is an overall broadening observed in the X-ray peak widths in 1, 2, and 3 compared to the Pb-deficient parent phases. It is observed that the X-ray peak widths of 2 is broad, while 3 displays narrow peak widths. It is found via strain analysis that the line broadening observed correlates with the strain in the lattice. © 2001 Academic Press

Key Words: **pyrochlore; Rietveld refinement; strain analysis; lead niobates; lead tantalates.**

I. INTRODUCTION

Studies of the $PbO–Nb_2O_5$ and the $PbO–Ta_2O_5$ systems have indicated the existence of a number of phases with structures apparently related to that of pyrochlore. The pyrochlore structure with the general formula $A_2B_2O_6O'$ is formed by a variety of ions and tolerates a high degree of nonstoichiometry on the O′ and the A cation sites (1). It is composed of a network of corner-sharing $(BO_6)_n$ polyhedra, with A cations filling the interstices. The structure consists of two types of cation coordinate polyhedra. The ideal pyrochlore structure crystallizes in the space group $Fd\bar{3}m$ (No. 227) with eight formula units per cell. The origin of the structure can be selected at the A, B, or the O site (1). Typically for lead niobates and tantalates, the assignment is that the A cations occupy the 16(*d*) site and are 8-coordinated with six equally spaced O anions and two additional axial O′ anions, while the smaller B cations occupy the 16(*c*) site and are 6-coordinated with all six anions at equal distances from the central cation. The oxygen anions O and O′ occupy the 48(*f*) $(x, \frac{1}{8}, \frac{1}{8})$ and 8(*b*) $(\frac{3}{8}, \frac{3}{8}, \frac{3}{8})$ sites, respectively. Thus a complete description of the three-dimensional arrangement of ions can be derived by the determination and refinement of only one positional parameter x of the O anion at 48(*f*) site (2). There are four lead niobate pyrochlore phases reported so far with stoichiometries, $Pb_{1.5}Nb_2O_{6.5}$, $Pb_2Nb_2O_7$, $Pb_{2.5}Nb_2O_{7.5}$, and $Pb_3Nb_2O_8$, all of which display varying degrees of nonstoichiometries at the A-site (3–7). However, among the lead tantalate pyrochlore phases ($Pb_{1.5}Ta_2O_{6.5}$, $Pb_{2.31}Ta_2O_{7.31}$, and $Pb_{2.44}Ta_2O_{7.44}$) the ideal composition $Pb_2Ta_2O_7$ is unstable but consists of an intergrowth between a Pb-deficient $Pb_{1.5}Ta_2O_{6.5}$ and a Pb-rich $Pb_{22}Ta_{18}O_{67}$ phase (8, 9). It is of interest to note that in all the above compositions the excess Pb is always found to be associated with the A-site. Recently, Sridhar *et al.* have synthesized solid solutions having a stoichiometry in the range $1.5PbO \cdot M_2O_5$ to $\sim 3\ PbO \cdot M_2O_5$ (M = Nb or Ta) at low temperatures ($\sim 500–600°C$) (10, 11). It was suggested that the excess lead might be at the B-site based on the broadening observed in the preliminary X-ray diffraction patterns. In order to explore the occupancy at the B-site explicitly, we have carried out detailed profile refinements using high-resolution powder X-ray diffraction data. To probe into the cause of the line broadening, the diffraction patterns have been subjected to strain analyses.

In the generally adopted theories (12), two types of structural line broadening are recognized to occur simultaneously: (i) particle-size broadening, caused by finite size of regions in the specimens diffraction incoherently with respect to each other and (ii) strain broadening due to varying displacements of the atom with respect to their reference positions. Normally particle-size broadening is negligibly small and hence ignored. The order dependence of the shape and width of line profiles is studied as a function of these model parameters.

[1] Address to whom correspondance should be addressed.

0022-4596/01 $35.00

TABLE 1
Results of EDAX Analyses for $Pb_2(M_{2-y}Pb_y)O_{7-\delta}$ ($0.0 < y < 0.8$; M = Nb, Ta)

	Relative concentration of M; M = Nb, Ta (at. %)	
y	Initial mixtures (Pb:M)	Powder samples (Pb:M)
0.49	60:40	64:36
0.60	60:40	64:36
0.75	69.31	71:29

II. EXPERIMENTAL

The compounds studied here were synthesized and supplied by Dr. Sreedhar (NCL, Pune, India). A detailed discussion on the low-temperature synthesis ($\sim 500-600^\circ$) of these are already described elsewhere (10, 11). Quantitative elemental analyses on all samples were carried out on a JEOL JSM-840 EDAX using Oxford instrument for X-ray analysis software in order to confirm the composition of the metal ions.

High-resolution X-ray diffraction data on $Pb_2Nb_{1.51}Pb_{0.49}O_{6.30}$ (**1**), $Pb_2Ta_{1.4}Pb_{0.6}O_{6.21}$ (**2**), and $Pb_2Ta_{1.25}Pb_{0.75}O_{6.57}$ (**3**) were collected on a STOE/STADI-P X-ray powder diffractometer with germanium monochromated Cu$K\alpha_1$ ($\lambda = 1.54056$ Å) radiation from a sealed tube X-ray generator (20 kV, 25 mA) in the transmission geometry. The samples were rotated during data collection to minimize preferred orientation effect, if any. The data were recorded on a linear PSD. The X-ray data were measured in the range $2\theta = 3$ to 78.60° in steps of 0.02° with 6 s exposure time per step at room temperature.

III. RESULTS AND DISCUSSION

Table 1 gives the results from the EDAX measurements, indicating that the ratio of the metal ions calculated nearly correspond to that of the ions taken initially for syntheses.

a. Profile Refinements

The trial and error indexing program TREOR (13) was used to index all the X-ray patterns. The compounds belong to the cubic system, space group $Fd\bar{3}m$, No. 227. The positional coordinates for the starting model for Rietveld refinements were taken from the published results on the pyrochlore $Pb_{1.5}Ta_2O_{6.5}$ (7). The GSAS (14) package is employed in all the calculations. The profiles were fitted using a pseudo-Voigt function that has three Gaussian and two Lorenztian coefficients. A cosine-Fourier function consisting of three to seven coefficients was used to define the background. The coordinate of the oxygen atom in the 48(f) position was first refined to convergence (All heavy atoms are in special positions in this space group), holding the occupancy and the thermal parameters fixed. Then the occupancies of Pb and M (Nb or Ta) were refined keeping the overall occupancy for the site fixed. Isotropic thermal parameters were then refined alternately with the occupancies. Since the refinements remained stable even after the oxygen occupancies were allowed to refine and the values obtained were in agreement with the limits of the expected values, it was discerned to accept the refined occupancy values. However, a detailed neutron diffraction study would ascertain the oxygen occupancy values with a higher degree of confidence. Details of the crystal data and refinements are given in Table 2.

TABLE 2
Crystal Data for $Pb_2(M_{2-y}Pb_y)O_{7-\delta}$; ($0 < y < 0.8$), M = Nb or Ta

Formula	$Pb_2Nb_{1.51}Pb_{0.49}O_{6.30}$	$Pb_2Ta_{1.4}Pb_{0.6}O_{6.21}$	$Pb_2Ta_{1.25}Pb_{0.75}O_{6.57}$
Formula weight	768.184	899.816	903.227
Color	Yellow	Yellow	Yellow
Space group	$Fd\bar{3}m$	$Fd\bar{3}m$	$Fd\bar{3}m$
Z	8	8	8
λ(Å)	1.54056	1.54056	1.54056
2θ	$3^\circ-78.60^\circ$	$3^\circ-78.60^\circ$	$3^\circ-78.60^\circ$
No. of reflections	30	29	29
No. of structural parameter	10	10	10
a (Å)	10.762(1)	10.744(1)	10.757(2)
V(Å^3)	1246.46(20)	1240.22(20)	1244.73(30)
R_{wp} (%)	11.84	10.60	9.98
R_p (%)	9.02	8.25	7.46
R (I, hkl) (%)	3.91	4.31	4.54
No. of data points	3781	3781	3781

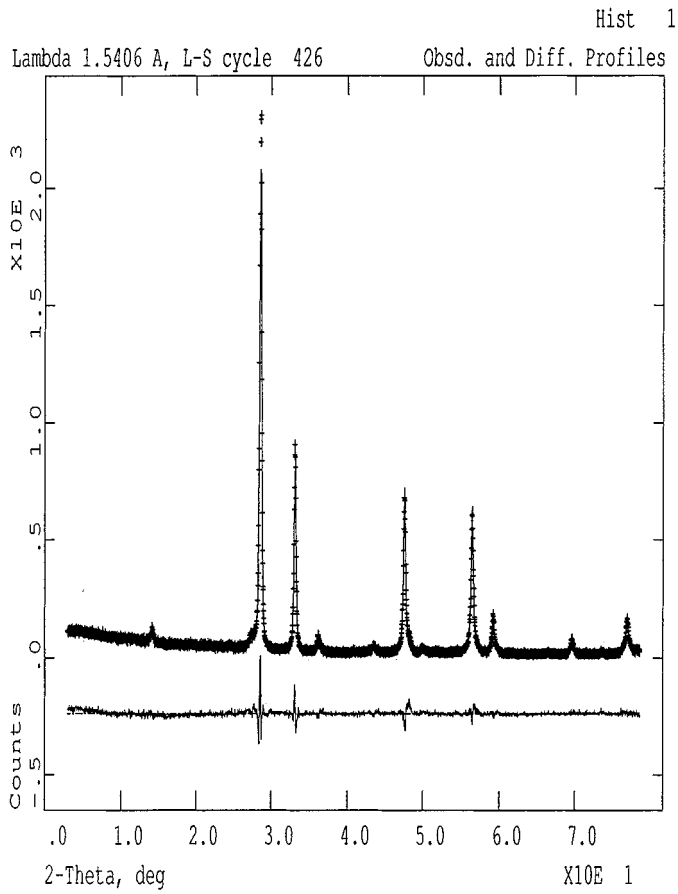

FIG. 1. Observed, calculated, and difference X-ray diffraction pattern of (**1**).

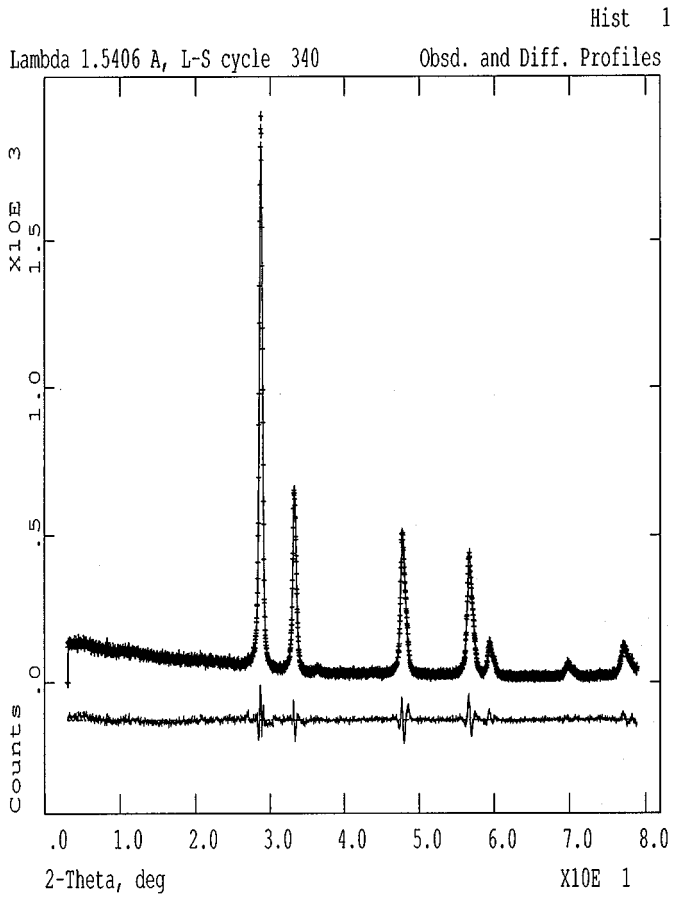

FIG. 2. Observed, calculated, and difference X-ray diffraction pattern of (**2**).

The structure reports on the lead antimonate pyrochlore Pb_2 $(Sb_{2-x}Pb_x)O_{7-\delta}$ and lead ruthenate pyrochlore Pb_2 $(Ru_{2-x}Pb_x)O_{7-\delta}$ (15, 16) suggest the presence of Pb^{4+} in the B-site. The lattice param eters *a*, for these two cases are 10.66 and 10.58 Å, respectively. These values are less than the *a* parameter values found in **1**, **2**, and **3**. It may be argued that this small difference in the lattice parameter is due to the differences in the ionic radii of the M^{5+} (Nb or Ta) and Sb^{5+} cations (17). Hence, it may be conjectured that the oxidation state of Pb in the B-site is 4+.

The observed, difference, and calculated patterns of all the three phases are shown in Figs. 1, 2, and 3. Tables 3a–3c list the final positional coordinates along with isotropic thermal parameters and Table 3d lists the bond lengths for all the phases. Figure 4 shows the octahedral coordination at the B site.

The Rietveld refinement results suggest the formation of a cubic pyrochlore solid solution with partial occupancy of Pb in the B-site leading to the formula Pb_2 $(M_{2-y}Pb_y)$ $O_{7-\delta}(0.0 < y < 0.8; M = \text{Nb or Ta})$. It is observed from the X-ray patterns that there is a significant broadening of the peaks in **2** compared to that seen in **3** and the parent compound (Fig. 5).

Sreedhar *et al.* (10) have observed that a cubic solid solution with part of the Pb in the B-site was formed in Nb pyrochlores for the sample with a PbO/Nb_2O_5 molar ratio of 2. Also it was observed that a minor amount of unreacted PbO was present when the PbO/Nb_2O_5 molar ratio was raised 3.5, suggesting that the maximum ratio is limited to 3.5. In case of the $PbO–Ta_2O_5$ system, the diffraction lines show significant broadening for the molar ratio $\lesssim 2.0$, while for the higher molar ratios (>2.3), the peak widths are narrowed. At this stage, a strain analysis was undertaken to evaluate these features.

b. Strain Analysis

A generally applicable one-dimensional model based on the distortion of the lattice (18, 19) has been used to obtain the average microstructural parameters like crystal size and strain along different directions of the lattice employing individual (*hkl*) reflections. The corrected experimental

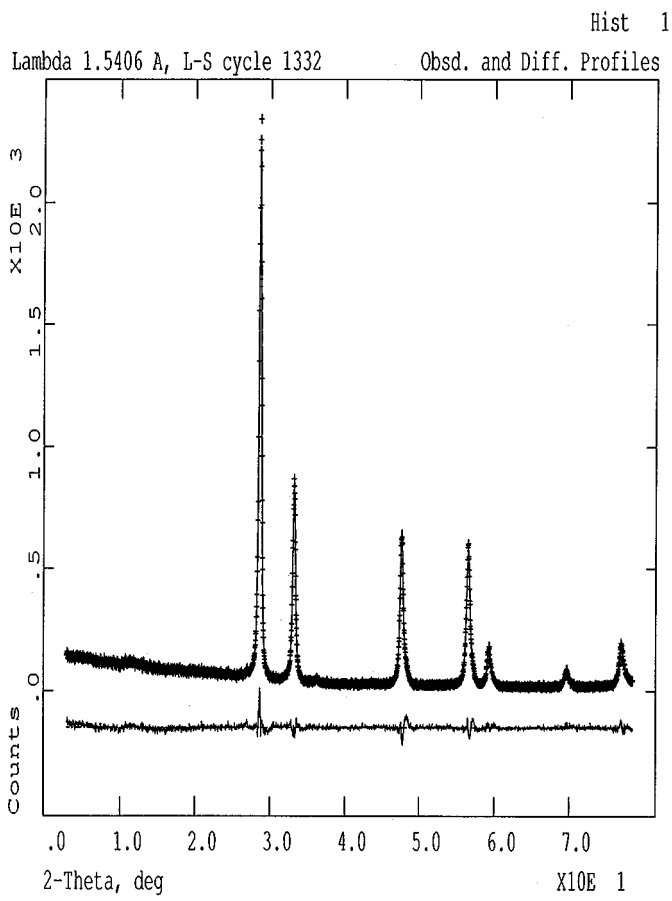

FIG. 3. Observed, calculated, and difference X-ray diffraction pattern of (**3**).

TABLE 3

Atom	Site	x	y	z	O	U_{iso} (Å^2)
(a) Final atomic coordinates from powder X-ray data at 298 K for $Pb_2Nb_{1.51}Pb_{0.49}O_{6.30}$						
Pb(1)	16(d)	0.5	0.5	0.5	1.000(5)	0.0335(10)
Nb(1)	16(c)	0.0	0.0	0.0	0.753(6)	0.01287(11)
Pb(2)	16(c)	0.0	0.0	0.0	0.2426(6)	0.01287(11)
O(1)	48(f)	0.3171(11)	0.125	0.125	1.000	0.04711(5)
O(2)	8(b)	0.375	0.375	0.375	0.305(51)	0.04711(5)
(b) Final atomic coordinates from powder X-ray data at 298 K for $Pb_2Ta_{1.40}Pb_{0.60}O_{6.21}$						
Pb(1)	16(d)	0.5000	0.5	0.5	1.000(3)	0.0224(1)
Ta(1)	16(c)	0.0000	0.0	0.0	0.702(81)	0.0217(1)
Pb(2)	16(c)	0.0000	0.0	0.0	0.299(81)	0.0217(1)
O(1)	48(f)	0.3356(7)	0.125	0.125	1.000	0.0285(5)
O(2)	8(b)	0.375	0.375	0.375	0.210(10)	0.0285(5)
(c) Final atomic coordinates from powder X-ray data at 298 K for $Pb_2Ta_{1.25}Pb_{0.75}O_{6.57}$						
Pb(1)	16(d)	0.5000	0.5	0.5	1.000(1)	0.0179(9)
Ta(1)	16(c)	0.0000	0.0	0.0	0.625(2)	0.0168(1)
Pb(2)	16(c)	0.0000	0.0	0.0	0.375(2)	0.0168(1)
O(1)	48(f)	0.3206(15)	0.125	0.125	1.000	0.0524(3)
O(2)	8(b)	0.375	0.375	0.375	0.448(10)	0.0524(3)

(d) Bond distances (Å) in $Pb_2(M_{2-y}Pb_y)O_{7-\delta}$ $(0.0 < y < 0.8)$; M = Nb or Ta

Bond distance (Å)	$Pb_2Nb_{1.51}Pb_{0.49}O_{6.30}$	$Pb_2Ta_{1.4}Pb_{0.6}O_{6.21}$	$Pb_2Ta_{1.25}Pb_{0.75}O_{6.57}$
(Pb–O(1)) × 2	2.330(1)	2.329(6)	2.330(9)
(Pb–O(2)) × 6	2.738(8)	2.709(11)	2.711(9)
(M/Pb–O(2)) × 6	2.035(4)	2.048(6)	2.046(8)
M = Nb or Ta			

Note. U_{iso} is the isotropic thermal parameter.

X-ray profile that was used for Rietveld analysis was matched with the simulated profile using the equations

$$I(s) = I_{N-1}(s) + I'_N(s),$$

where $I'_N(s)$ is the modified intensity for the probability peak centered at D (= Nd_{hkl}). It has been shown that

$$I'_N(s) = (2\,a_N/D\pi^{1/2})\exp(idNs)[1 - a_N s\{2D(a_N s) + i\pi^{1/2}\exp(-a_N^2 s^2)\}],$$

where $a_N^2 = Nw^2$ and $D(a_N s)$ is the Dawson's integral or the error function with purely complex argument and can be easily computed. N is the number of unit cells counted in a direction perpendicular to the (hkl) Bragg plane. The experimental profile between s_o and $s_0 + s_o/2$ (or s_o and $s_o + B/2d$, if there is truncation of the profile $B < 1$) is matched with the corresponding simulated order of reflection between s_o and $s_o/2$ (or s_o and $s_o + B/2d$) using a one-dimensional distorted model for various values of N and g to minimize the difference between calculated and experimental normalized intensity values. SIMPLEX, a multi-dimensional algorithm is used for minimization. Tables 4a–4c and 5a–5c list the values of the microstructural parameters N, g, and hence D (in Å) along with their standard deviations obtained for the X-ray reflections of **1**, **2**, **3**, and the parent phases. The estimated enthalpy α^* ($= N^{1/2}g$), which physically implies that the growth of the crystals in a particular material is controlled appreciably by the value of g in the net plane structure (20, 21). The corrected experimental X-ray profile that was used for Rietveld analysis was matched with the simulated profile before computing the microstructural parameters as described earlier. A better perspective is to project the crystal size values obtained in terms of (hkl) planes on to a two-dimensional plot, with the D_{hkl} value plotted along the X-axis. It is found that the 222 plane is common in all these phases, which helps in projecting the crystal size on a two-dimensional plane. Further if D_{222} is considered to be the major axis plotted

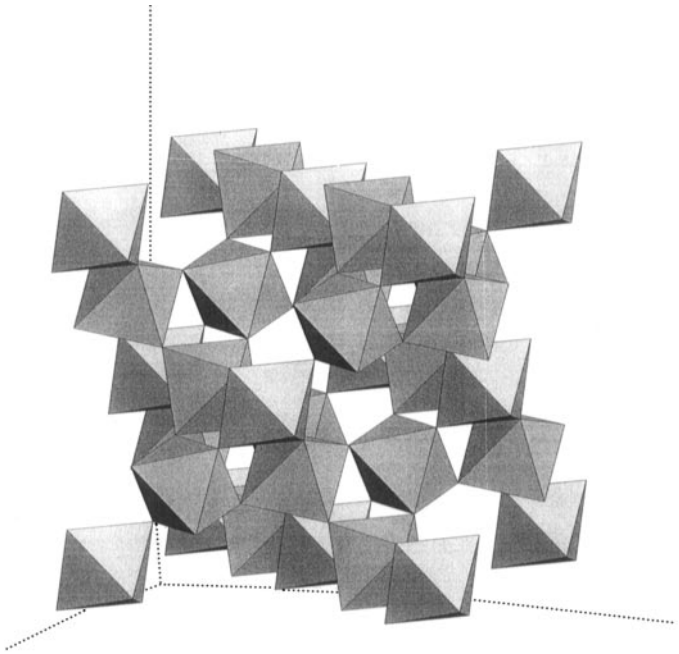

FIG. 4. MO_6 (M = Nb or Ta) octahedra viewed down the c axis.

along the X direction of an ellipse then the minor axis can be determined by an iterative procedure based on the expression

$$(2D_{hkl}^2) = (\cos\varphi/Y)^2 + (\sin\varphi/X)^2,$$

where φ is the angle between the hkl planes. The best value of Y obtained based on the iterative procedure is plotted along the minor axis and denoted as $Y_{\min}$ (Tables 4a–4c, 5a and 5b; Figs. 6 and 7). The Ta phases show that the crystallite size and volume decrease in the order **2** > **3** > $Pb_{1.5}(Ta_2)O_{7-\delta}$ (Fig. 6), which explains that reason for broaden-

TABLE 4

hkl	*N*	*g* (%)	*D* (nm)	α*
	(a) Microcrystalline parameters of $Pb_{1.5}(Ta_2)O_{7-\delta}$			
111	34.4(3)	4.4(1)	21.01	0.257
222	31.3(2)	1.7(1)	9.57	0.096
444	31.3(5)	0.9(1)	4.79	0.048
400	100.2(13)	3.9(1)	26.55	0.395
800	145.7(2.6)	2.1(1)	19.29	0.256
662	145.9(3)	2.3(1)	17.74	0.274
440	152.4(2.8)	3.3(1)	28.55	0.412
622	168.1(1.2)	2.2(1)	28.86	0.281
$\alpha^*_{avg} = 0.0.328$; $X = 9.57$ nm, $Y_{min} = 8.85$ nm, $Y_{min}/X = 0.924$; std = 2.8%; $D_{100} = D_{010} = D_{001} = 18.62$ nm; volume (nm^3) = 6458.				
	(b) Microcrystalline parameters of (**2**)			
222	50.4(1)	5.3(1)	15.63	0.377
444	50.1(8)	3.9(1)	7.79	0.281
400	46.9(5)	5.3(1)	12.63	0.363
800	41.2(5)	4.5(1)	5.55	0.291
662	201.0(8)	1.8(1)	24.82	0.249
440	46.5(6)	5.5(1)	8.86	0.372
622	59.1(7)	3.8(1)	9.61	0.291
$\alpha^*_{avg} = 0.252$; $X = 15.63$ nm, $Y_{min} = 4.72$ nm, $Y_{min}/X = 0.302$; std = 2.7%; $D_{100} = D_{010} = D_{001} = 15.04$ nm; volume (nm^3) = 3399.				
	(c) Microcrystalline parameters of (**3**)			
222	59.4(3)	4.4(1)	18.49	0.342
444	66.1(9)	2.7(1)	10.3	0.219
400	58.8(6)	4.9(1)	15.9	0.372
800	64.8(12)	2.2(1)	8.73	0.178
662	89.5(3)	2.3(1)	11.07	0.219
440	68.2(5)	4.5(1)	13.02	0.368
622	69.7(5)	2.9(1)	11.34	0.241
$\alpha^*_{avg} = 0.274$; $X = 18.49$ nm, $Y_{min} = 4.96$ nm, $Y_{min}/X = 0.268$; std = 1.6%; $D_{100} = D_{010} = D_{001} = 16.06$ nm; volume (nm^3) = 4145.9.				

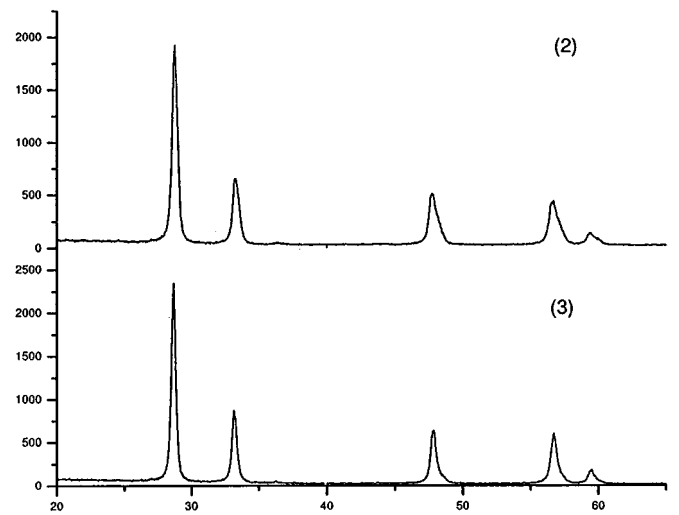

FIG. 5. Comparison of the X-ray peak widths for samples (**2**) and (**3**).

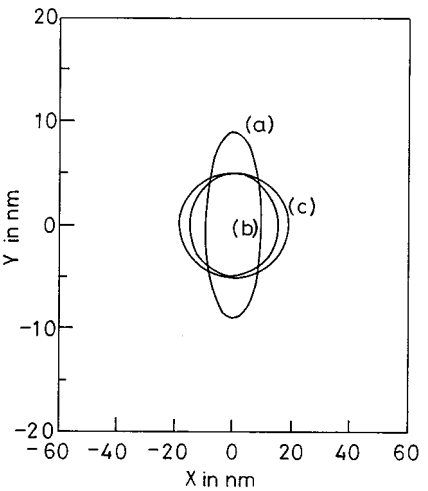

FIG. 6. Comparison of the crystallite shape for (a) $Pb_{1.5}Ta_2O_{7-\delta}$, (b) (**2**), (c) (**3**).

TABLE 5

hkl	*N*	*g* (%)	*D* (nm)	α^*
	(a) Microcrystalline parameters of $Pb_{1.5}(Nb_2)O_{7-\delta}$			
111	60.8(8)	4.6(1)	37.09	0.257
222	60.0(6)	2.1(1)	18.41	0.096
444	60.3(9)	1.4(1)	9.25	0.048
400	159.8(56)	3.4(1)	42.45	0.395
800	150.1(2)	1.1(1)	19.93	0.256
331	150.1(62)	3.1(1)	36.59	0.376
662	150.0(1.5)	1.1(1)	18.27	0.124
440	225.6(6.8)	2.9(1)	42.27	0.431
511	203.6(43)	2.7(1)	41.62	0.385
311	120.3(35)	3.7(1)	38.57	0.405
622	120.3(25)	1.6(1)	19.27	0.175
$\alpha^*_{avg} = 0.279$; $X = 18.41$ nm, $Y_{min} = 13.65$ nm, $Y_{min}/X = 0.744$; std = 3.5%; $D_{100} = D_{010} = D_{001} = 32.63$ nm; volume (nm^3) = 34153.				
	(b) Microcrystalline parameters of (**1**)			
222	139.4(35)	3.6(1)	43.51	0.428
444	200.8(9)	1.4(1)	31.3	0.201
400	159.8(56)	3.4(1)	43.23	0.425
800	159.0(2)	1.1(1)	21.47	0.139
311	119.9(23)	3.7(1)	75.18	0.408
662	147.9(3.3)	1.6(1)	24.11	0.199
331	150.1(6.2)	3.0(1)	37.23	0.369
662	200.9(26)	1.3(1)	24.87	0.174
440	225.6(68)	2.9(1)	43.09	0.405
$\alpha^*_{avg} = 0.308$; $X = 43.51$ nm, $Y_{min} = 15.94$ nm, $Y_{min}/X = 0.366$; std = 5.8%; $D_{100} = D_{010} = D_{001} = 49.03$ nm; volume (nm^3) = 117852.				

ing of lines in **2** compared to the other two compositions. The trend that is observed in the Nb compositions though is seen to be (Fig. 7) different; i.e., there is a considerable increase in volume and crystallite size in **1** compared to the Pb-deficient parent phase. Also the average value of α is minimum for the parent phases, indicating phase stabilization in these samples compared to the compositions **1**, **2**, and **3**.

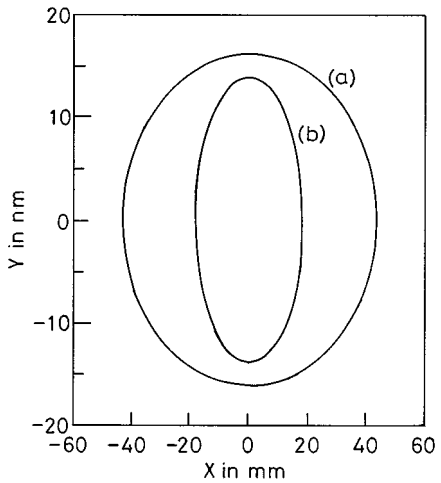

FIG. 7. Comparison of the crystallite shape for (a) $Pb_{1.5}Nb_2O_{7-\delta}$ and (b) (**1**).

IV. CONCLUSIONS

The Rietveld refinements clearly establish that in substituted lead pyrochlore of the type $Pb_2(M_{2-y}Pb_y)O_{7-\delta}$ ($0 < y < 0.8$; M = Nb or Ta) the excess Pb is present at the B site. The broadening of the X-ray peaks in **1**, **2**, and **3** compared to the parent phases causes strain in the lattice due to the addition of Pb in the B site. Strain analysis supports this observation. Compositions **1**, **2**, and **3** are less stabilized than the parent phase. The oxidation state of Pb in the B site has been conjectured to be 4+ based on comparative studies.

REFERENCES

1. R. A. McCauley, *J. Appl. Phys.* **51**(1), 290 (1980).
2. B. J. Kennedy and T. Voigt, *J. Solid State Chem.* **126,** 261 (1996).
3. R. S. Roth, *J. Res. Natl. Bur. Stand.* **62**(1), 27 (1959).
4. S. Kemmler-Sack and W. Rudorff, *Z. Anorg. Allg. Chem.* **344**(1–2), 23 (1966).
5. H. Brusset, M. H. Gillier-Pandraud, R. Mahe, and S. D. Voliotis, *Mater. Res. Bull.* **6,** 413 (1971).
6. H. Brusset, R. Mahe, and U. A. Kyi, *Mater. Res. Bull.* **7**(10), 1061 (1972).
7. O. Yamaguchi and Y. Mukaida, *J. Am. Ceram. Soc.* **73**(6), 1705 (1990).
8. H. G. Scott, *J. Solid State Chem.* **43,** 131 (1982).
9. N. Menguy, F. Thuries, and C. Caranoni, *J. Solid State Chem.* **126,** 253 (1996).
10. K. Sreedhar and A. Mitra, *J. Am. Ceram. Soc.* **82**(4), 1070 (1999).
11. K. Sreedhar and A. Mitra, *J. Am. Ceram. Soc.* **83**(2), 418 (2000).
12. B. E. Warren, "X-Ray Diffraction," Chap. B, p. 264. Addison-Wesley, Reading, MA, 1969.
13. P. Werner, *Z. Kristallogr.* **120,** 385 (1964).
14. A. C. Larson and R. B. von Dreele, "Los Alamos Laboratory Report LA-UR-86-748." Los Alamos, NM, 1987.
15. G. Burchard and W. Rudorff, *Z. Anorg. Allog. Chem.* **447,** 149 (1978).
16. R. A. Beyerlein, H. S. Horowitz, and J. M. Longo, *J. Solid State Chem.* **72,** 2 (1988).
17. R. D. Shannon, *Acta Crystallogr. A* **32,** 751 (1976).
18. K. Sooryanarayana, R. Somashekar, and T. N. Guru Row, *Solid State Ionics* **104,** 319 (1997).
19. R. Somashekar and H. Somashekarappa, *J. Appl. Crystallogr.* **30,** 147 (1997).
20. R. Hosemann, *Prog. Coll. Sci.* **77,** 15 (1988).
21. R. Hosemann and A. M. Hindeleh, *J. Mater. Sci.* **26,** 5127 (1991).